IEEE Access
Multidisciplinary | Rapid Review | Open Access Journal

SPECIAL SECTION ON ADVANCES IN MACHINE LEARNING AND COGNITIVE COMPUTING FOR INDUSTRY APPLICATIONS

Received March 15, 2020, accepted April 1, 2020, date of publication April 13, 2020, date of current version April 28, 2020.

Digital Object Identifier 10.1109/ACCESS.2020.2987349

A Machine Learning Based Connectivity Restoration Strategy for Industrial IoTs

JIONG WANG[1,2,3], HUA ZHANG[1,2,3], ZHIQIANG RUAN[1,2,3], TAO WANG[1,2,3], AND XIAODING WANG[4]

[1]College of Computer and Control Engineering, Minjiang University, Fuzhou 350108, China
[2]Fujian Provincial Key Laboratory of Information Processing and Intelligent Control, Minjiang University, Fuzhou 350108, China
[3]Industrial Robot Application of Fujian University Engineering Research Center, Minjiang University, Fuzhou 350108, China
[4]Fujian Provincial Key Laboratory of Network Security and Cryptology, College of Mathematics and Informatics, Fujian Normal University, Fuzhou 350117, China

Corresponding authors: Tao Wang (eetaowang@gmail.com) and Xiaoding Wang (ttclarkwang1982@sina.com)

This work was supported in part by the National Natural Science Foundation of China under Grant 61702103, Grant 61871204, and Grant 61703195, in part by the Guiding Project of Fujian Science and Technology Department under Grant 2019H0026, in part by the Fujian Natural Science Foundation under Grant 2019J01756, in part by the Fujian Science and Technology Department Project under Grant 2017J01768, in part by the Education and Research Project for Young and Middle-aged Teachers in Fujian Province under Grant JT180405, in part by the Fujian Provincial Key Laboratory of Information Processing and Intelligent Control (Minjiang University) under Grant MJUKF-IPIC201809, in part by the Industrial Robot Application of Fujian University Engineering Research Center (Minjiang University) under Grant MJUKF-IRA1906, and in part by the Fuzhou Technology Planning Program Grant 2018-G-96.

ABSTRACT The connectivity restoration has significance for Industrial IoTs (IIoTs). If the connectivity is compromised, mobile data collectors can be deployed to restore the connectivity. The aggregation ratio, which is the proportion of data successfully delivered to the sink over all data, is considered as a crucial index. However, previous works only consider the travel distance, the load balance, the latency and the energy cost over the aggregation ratio. In this paper, a machine learning based connectivity restoration strategy CRrbf, that utilizes a Radial Basis Function Neural Network (RBFNN) along with an Unscented Kalman Filter (UKF), is proposed to maximize the aggregation ratio meanwhile reduce the energy cost. The theoretical analysis and simulation results indicate that CRrbf outperforms both distance based strategies and terrain based strategies in the aggregation ratio, the network latency and the network throughput. And the energy cost of CRrbf is less than that of distance based strategies.

INDEX TERMS IIoTs, connectivity restoration, machine learning.

I. INTRODUCTION

Services provided by an Industrial Internet of Things (IIoTs) rely on connectivity which enables inter-connect smart objects to exchange data and achieve individual and/or network objectives. And connectivity technologies have the potential of driving the next industrial revolution [1]. That suggests the significance of connectivity [2]–[6]. Be specific, smart devices of IIoTs link to access points through wireless personal area networks [7] and eventually connect to wide area networks [8]. However, the connection could be compromised by nature disasters [9], [10] or human sabotages [11], [12] that results in connectivity loss. Then, one should deploy relay devices, i.e., Mobile Data Collectors (MDCs), for connectivity restoration.

The associate editor coordinating the review of this manuscript and approving it for publication was Jiong Jin.

Connectivity restoration strategies were initially designed for wireless networks, among which MDCs are employed to provide intermittent connection among components. The ratio of successful data transmissions from sensors to the base station is called the aggregation ratio, by which Liu *et al.* [13] characterize the data deliverability of greedy routing. Such ratio deemed as a crucial index due to the fact that the connectivity is restored to guarantee the data aggregation. Although MDCs enable to collect data from an entire component, the number of which are insufficient. That suggests each MDC should recursively collect data over a certain area. However, the MDC tour design is NP-hard as the Traveling Salesman Problem (TSP). There exist a number of Distance Based Strategies (DBS) [14]–[21] that aim to find the shortest travel distance to serve specific purposes over the aggregation ratio. On the other hand, terrains of realistic environments (e.g., mountain, river, forest, swamp, etc.) make

TABLE 1. Comparison of contemporary heuristic algorithms.

Algorithm	Aggregation ratio	Complexity
CRrbf (this paper)	$\frac{1}{1+\theta}$	$O(n^2 \log n!)$
LEEF [15]	$\frac{1}{\frac{4}{3}(1+\theta)}$	$O(n^2 logn)$
RCR [16]	$\frac{1}{\frac{4}{3}(1+\theta)}$	$O(n^2)$
MIMSI [18]	$\frac{1}{\frac{4}{3}(1+\theta)}$	$O(n^4)$
IDM-kMDC [21]	$\frac{1}{\frac{4}{3}(1+\theta)}$	$O(n^4 \log n)$
FeSMoR [20]	$\frac{1}{\frac{4}{3}(1+\theta)}$	no available
MINDS [17]	$\frac{1}{\frac{4}{3}(1+\theta)}$	$O(n \log n)$
ToCS [19]	$\frac{1}{\frac{4}{3}(1+\theta)}$	no available
CISIL [14]	$\frac{1}{\frac{n}{3l_m}(1+\theta)}$	$O(n^4)$
HRSRT [22]	$\frac{1}{\frac{2.325}{\alpha}(1+\theta)}$	$O(n^3)$
ReBAT [23]	$\frac{1}{\frac{3.1}{\alpha}(1+\theta)}$	no available

TABLE 2. Notions.

Symbols	Descriptions
C_i	The ith component
l_m	Number of MDCs
s_i^*	Collection node of C_i
s_i	Sinking point of group G_i
v	Velocity of each MDC
r	Communication rage of s_i
θ	Tolerable data loss rate
Buf_{s_i}	Buffer size of node s_i
DCR_{s_i}	Data collection rate of node s_i
d_{s_i,s_j}	Euclidean length of edge $s_i s_j$
P_{s_i,s_j}	Path between s_i and s_j
$\omega(G)$	Weight of graph G
H_G	Hamilton cycle of graph G
$L(G)$	Euclidean length of graph G
AR_A	Aggregation ratio of algorithm A
$E(G)$	Energy cost of MDC travelling along G
E_A	Energy cost of algorithm A

difficulties to data collection that results in more energy cost. To restore the connectivity in realistic environments, plenty of works [22]–[28], called Terrain Based Strategies (TBS), are proposed to diminish terrain influences for energy saving.

Our Contribution: In this paper, we propose a machine learning based strategy CRrbf that deploys a limited number of MDCs to restore the connectivity. In general, CRrbf consists of the UKF-RBFNN based Data Collection Rate (DCR) prediction and the corresponding greedy grouping. The details of our contributions are listed as follows. And we give the comparison of contemporary heuristic algorithms in Table 1 in terms of aggregation ratio and complexity, where $\alpha = \frac{Buf_{s_i} cv^2 r_{min} elev_{min}(1+\theta)}{DCR_{s_i} E^*} < 1$, c is the energy factor proportional to the travelling speed v, E^* is the optimal energy cost, r_{min} and $elev_{min}$ represent the minimal risk and the minimal elevation of the entire deployment area, respectively.

1) To restore the connectivity meanwhile improve the aggregation ratio, CRrbf first employs a Radial Basis Function Neural Network (RBFNN) trained by the Unscented Kalman Filter (UKF) to predict the data collection rate for each node. Then, CRrbf designs each MDC tour with consideration of travel distance, buffer size and data collection rate to confine the travel time of each MDC to that of filling up the buffer. Thus, the aggregation ratio is significantly improved. More importantly, MDC tours discovered by CRrbf mitigate terrain influences on data collection such that energy cost is reduced.
2) The theoretical proofs and simulation results indicate that SR_{CRrbf} is no less than $\frac{1}{1+\theta}$, which is $\frac{1}{4(1+\theta)}$ higher than that of any DBSs or TBSs, where θ represents the tolerable data loss rate. And the energy cost of CRrbf is lower than any DBSs. Furthermore, CRrbf is proved to have a less network latency and a better network throughput while compared with any DBSs or TBSs.

The rest of the paper is organized as follows. The system model is introduced in Section II. The strategies are elaborated in Section III. The theoretical analyses on complexity, aggregation ratio, network latency and network throughput of CRrbf are also given in this Section. The validation results are presented in this Section as well. Related work is covered in Section V. We conclude this paper in Section VI.

II. SYSTEM MODEL

Consider a IIoTs network composed of a set of homogeneous devices. Each IIoTs device represents a surveillance camera or a sensor dedicated for a certain type of application. Each device s_i has a communication rage r, a buffer Buf_{s_i} and a data collection rate DCR_{s_i}. Each link exists between a pair of s_i and s_j, only if the distance of which is less or equal to r. Once the connectivity is lost, MDCs are assigned for data collection, each of which possess a powerful antenna to upload data directly to the sink. Thus, the MDC tour should be designed to provide intermittent connection for fault tolerant IIoTs [29], [30]. In order to maintain the aggregation ratio meanwhile minimize the energy cost during the connectivity restoration. Terrain influences should be quantified.

The grid of equal size is applied for quantifying terrain influence. More specific, each cell c_i is associated with a weight referring to a certain terrain

$$\omega(c_i) = dist(c_i) \times r(c_i) \times elev(c_i), \tag{1}$$

where $dist(c_i)$, $r(c_i)$ and $elev(c_i)$ stands for the distance, the risk and the elevation a MDC travels through c_i, respectively. According to (1), we give the weight of a path P_{s_i,s_j} as follows:

$$\omega(P_{s_i,s_j}) = \sum_{c_k \in P_{i,j}} \omega(c_k). \tag{2}$$

We denote $\tilde{P}_{s_i,s_j}$ the minimum weight path between s_i and s_j throughout the paper. Let T_i be a MDC tour. According to (2), $\omega(T_i)$ thus is given as follows:

$$\omega(T_i) = \sum_{P_{s_i,s_j} \in T_i} \omega(P_{s_i,s_j}). \tag{3}$$

Then, the weight of a tour $T = \cup T_i$ is given by $\omega(T) = \sum_{i=1}^{l_m} \omega(T_i)$. However, how to find the minimum weight paths is still a problem. In fact, it can be modelled into a minimum weight Steiner tree problem. The reason for that is since each collection node is located within a cell, eight neighbor cells of which are candidate positions for Steiner points. Accordingly, the polynomial time algorithm k-LCA [34] can be used to find minimum weight paths for each pair of sensors. Then, we define the energy cost $E^{tour}(T)$ of a tour T as follows:

$$E^{tour}(T) = \omega(T) \times c, \tag{4}$$

where $c \propto v$. It is obviously that the $E^{tour}(T)$ is proportional to the terrain influence. On the other hand, if a MDC visits each component $C_i \in T_i$, then the data of which is collected at the collection node $s_i^* \in C_i$ first and eventually uploaded to the sink at a sinking point $s_i' \in T_i$. Then, the energy cost of data transmission at a sensor $s_j \in C_i$ is calculated as:

$$E^{trans}(s_j, s_i^*) = k \times d_{s_j, s_i^*}^2 \tag{5}$$

where k is a constant coefficient related to the power of a sensor and the amount of data collected as well. According to (3), (4) and (5), the energy cost $E^{sink}(T_i)$ during the sinking process is given as follows:

$$E^{sink}(T_i) = E^{trans}(s_i', sink) + \sum_{C_i \in T_i} E^{trans}(C_i), \tag{6}$$

where $E^{trans}(C_i) = \sum_{s_j \in C_i} E^{sink}(s_j, s_i^*)$. Thus, the total sinking cost is given by $E^{sink}(T) = \sum_{i=1}^{l_m} E^{sink}(T_i)$. According to (6), the total energy cost of the tour T constructed by algorithm A is given by

$$E_A(T) = E^{sink}(T) + E^{tour}(T). \tag{7}$$

Note that $E^{tour}(T)$ is affected by both of terrains and travelling distances, while $E^{sink}(T)$ is distance-related. The terrain influence quantification is followed by MDC tour design which relies on the DCR prediction and corresponding grouping, the priority of which is the maximization of the aggregation ratio. To this end, the travel distance should be shortened. However, a path of the minimum energy cost may result in a detour with a longer distance. In this paper, we propose a UKF-RBF based Connectivity Restoration strategy CRrbf that consists of the terrain influence quantification, the DCR prediction and corresponding grouping.

Be specific, all representatives that serve as collection nodes chosen from components, should be located closely.Then, the terrain influences quantification is applied to calculate the energy cost for a MDC travelling along any edge between a pair of representatives. Meanwhile, an UKF-RBF is utilized to predict the DCR_{s_i} for all $s_i s \in C_i$ to determine the proper DCR for C_i, which is denoted by $DCR_{s_i^*}$. CRrbf design MDC tours to meet the constrain that the time gap of visiting the a component twice should be less or equal to that of filling a buffer $Buf_{s_i^*}$ for aggregation ratio improvement. Furthermore, the MDC tours should be of least energy cost. The flowchart of the CRrbf is given in Fig. 1.

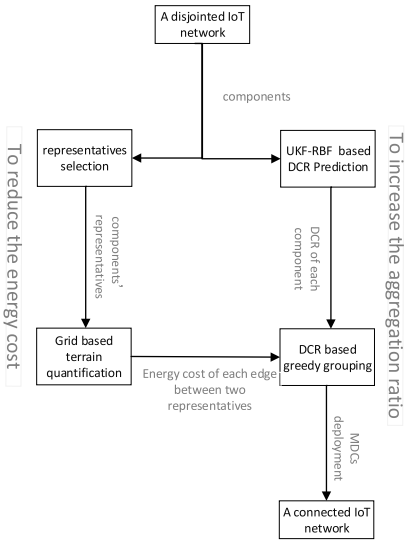

FIGURE 1. The flowchart of CRrbf.

III. THE PROPOSED STRATEGY

A. UKF-RBFNN BASED DCR PREDICTION

Since each sensor has a limited buffer size, if the buffer is filled up, new data can be stored such that the aggregation ratio drops. That implies the significance of a proper DCR_{s_i}, where $s_i \in C_i$. There exists a series of machine learning based strategies that utilize neural network [31]–[33] for prediction and classification. We apply a multiple fading factors strong tracking UKF to train the RBFNN in order to predict the DCR_{s_i}. For simplicity, we use X_t to denote the state vector of s_i at a time slot t, while Y_t denotes the predicted DCR_{s_i}.

Let the RBF neural network has $3m$ input nodes and only 1 output node such that state vector X_k formed by parameters of which is given by

$$X_k = [\omega_1, \ldots, \omega_m, c_1, \ldots, c_m, b_1, \ldots, b_m],$$

where ω_i denotes the weight of ith output layer, c_i and b_i represent the center and the variance of the ith hidden layer with $1 \leq i \leq m$. And the state function and observation function is given as follows:

$$\begin{cases} X_k = X_{k-1} + v_{k-1}, \\ Z_k = h(X_k, x_t) + e_k \end{cases}$$

where Z_k is the measurement value which is a real number, v_k and e_k represent the process noise and the measurement noise respectively, and $h(\cdot)$ consists of Gaussian kernel functions. Note that v_k and e_k are assumed to be uncorrelated white Gaussian noise such that $E(v_k) = E(e_k) = 0$, $E(v_k e_k^T) = 0$, $E(v_k v_k^T) = Q_k$, $E(e_k e_k^T) = R_k$, where Q_k and R_k are symmetric positive definite matrices. The prediction performed by MSTUKF-RBF are given as follows:

1. Predict the system state matrix, covariance matrix, and measurement matrix

$$\begin{aligned}
\chi_{i,k+1|k} &= \chi_{i,k|k} + v_k \\
\hat{X}_{k+1|k} &= \sum_{i=0}^{2L} \omega_i^m \chi_{i,k+1|k} \\
P_{k+1|k} &= \Lambda_{k+1} \sum_{i=0}^{2L} \omega_i^c [\chi_{i,k+1|k} - \hat{\chi}_{k+1|k}] \\
&\quad [\chi_{i,k+1|k} - \hat{\chi}_{k+1|k}]^T + Q_k \\
Z_{i,k+1|k} &= h(\chi_{i,k+1|k}, x(k+1)) + e_k \\
\hat{Z}_{k+1|k} &= \sum_{i=0}^{2L} \omega_i^m Z_{i,k+1|k}
\end{aligned} \tag{8}$$

where w_i^m represent the weight of predicted mean, $\Lambda_{k+1} = diag[\lambda_{1,k+1}, \lambda_{2,k+1}, \cdots, \lambda_{n,k+1}]$ (see Theorem 1).

2. Calculate the covariance matrix of the system and the Kalman gain

$$\begin{aligned}
P_{zz,k+1|k} &= \sum_{i=0}^{2L} \omega_i^c [Z_{i,k+1|k} - \hat{Z}_{k+1|k}][Z_{i,k+1|k} - \hat{Z}_{k+1|k}]^T \\
&\quad + R_k \\
P_{xz,k+1|k} &= \sum_{i=0}^{2L} \omega_i^c [\chi_{i,k+1|k} - \hat{X}_{k+1|k}][Z_{i,k+1|k} - \hat{Z}_{k+1|k}]^T \\
K_{k+1} &= P_{xz,k+1|k} P_{zz,k+1|k}^{-1}
\end{aligned}$$

3. Update the system state matrix and covariance matrix

$$\begin{aligned}
\hat{X}_{k+1} &= \hat{X}_{k+1|k} + K_{k+1}(Z_{k+1} - \hat{Z}_{k+1|k}) \\
P_{k+1} &= P_{k+1|k} - K_{k+1} P_{zz,k+1|k} K_{k+1}^T
\end{aligned}$$

4.Calculate the updated output of the hidden layer in the RBF

$$P_j(\hat{X}_k, x_t) = exp(\frac{-||x_t - c_j||^2}{2b_j^2}),$$

where $1 \le j \le m$, and P_j is the jth output of the hidden layer.

5. Calculate the output of the RBF

$$Y_t = \sum_{j=1}^{m} \omega_j P_j(\hat{X}_k, x_t),$$

where Y_t is the predicted DCR_{s_i} at time slot t. For each $s_i \in C_i$, the $DCR_{s_i^*}$ is chosen as follows:

$$DCR_{s_i^*} = \max\{DCR_{s_i}\}.$$

We give the following theorem for the choices of multiple fading factors.

Theorem 1: The diagonal matrix Λ of fading factors should be calculated as

$$\lambda_{i,k} = \begin{cases} \alpha_i c_k, & \alpha_i c_k > 1 \\ 1, & \alpha_i c_k \le 1, \end{cases} \tag{9}$$

where

$$c_k = \frac{tr[N_k]}{\sum_{i=1}^{n} \alpha_i M_k^{ii}}.$$

Proof: Zhou *et al.* [37] prove that the multiple fading factor matrix $\xi_k = diag[\xi_{1,k}, \xi_{2,k}, \cdots, \xi_{n,k}]$ of a Multiple Strong Tracking Extended Kalman Filter can be calculated as

$$\xi_{i,k+1} = \begin{cases} \alpha_i c_k, & \alpha_i c_k > 1 \\ 1, & \alpha_i c_k \le 1, \end{cases}$$

where

$$c_k = \frac{tr[N_k]}{\sum_{i=1}^{n} \alpha_i M_k^{ii}} \tag{10}$$

$$N_k = V_k - H_k Q_{k-1} H_k^T - R_k, \tag{11}$$

$$M_k = F_{k|k-1} P_{k-1|k-1} F_{k|k-1}^T H_k^T H_k = (M_k^{ij}), \tag{12}$$

$$V_{k+1} = \begin{cases} \gamma_1 \gamma_1^T, & k = 1 \\ \dfrac{\rho V_k + \gamma_{k+1} \gamma_{k+1}^T}{1+\rho}, & k \ge 1 \end{cases} \tag{13}$$

$$\frac{\partial f}{\partial \hat{x}_{k-1|k-1}} = F_{k|k-1}, \quad \frac{\partial h}{\partial \hat{x}_{k|k-1}} = H_k,$$

and $\rho \in (0, 1]$ is a forgetting factor usually chosen as 0.95. Since $X_k - \hat{X}_{k|k-1}$ is irrelevant to v_k, it can be deduced that

$$P_{xz,k|k-1}^l = P_{k|k-1}^l H_k^T. \tag{14}$$

As the Q_k is assumed to be a positive definite symmetric matrix, we have

$$H_k = [P_{xz,k|k-1}^l]^T [P_{k|k-1}^l]^{-1}, \tag{15}$$

where $P_{xz,k|k-1}^l$ denotes the cross-covariance between the predicted state and measurement and $P_{k|k-1}^l$ represents the prediction covariance without introducing fading factors. Substituting (15) into (11) yields

$$N_k = V_k - [P_{xz,k|k-1}^l]^T [P_{k|k-1}^l]^{-1} Q_{k-1} [P_{k|k-1}^l]^{-1} P_{xz,k|k-1}^l - R_k. \tag{16}$$

It is evident that

$$P_{k|k-1}^l = F_{k|k-1} P_{k-1|k-1} F_{k|k-1}^T + Q_{k-1}. \tag{17}$$

Substituting (15) and (17) into (12) yields

$$M_k = (P_{k|k-1}^l - Q_{k-1})[P_{k|k-1}^l]^{-1} [P_{xz,k|k-1}^l]^T [P_{k|k-1}^l]^{-1}. \tag{18}$$

Eventually, substituting (16) and (18) into (10) to calculate multiple fading factors as

$$\lambda_{i,k} = \begin{cases} \alpha_i c_k, & \alpha_i c_k > 1 \\ 1, & \alpha_i c_k \le 1, \end{cases}$$

where

$$c_k = \frac{tr[N_k]}{\sum_{i=1}^{n} \alpha_i M_k^{ii}}.$$

■

Note that the implementation of UKF requires a priori knowledge of both the process and measurement noise statistics. For most nonlinear systems, the process and measurement noise is time-varying, so it is essential to adaptively estimate both the noise statistics to improve UKF estimation and filtering performance. Generally, the measurement noise covariance matrix R is adapted based on the residual covariance matching method, while the process noise covariance Q is adapted based on the estimated R. We give the following theorem for process noise covariance Q adaption.

Theorem 2: The adaptive scaling factor μ_k for process noise covariance Q can be calculated as

$$\mu_k = \begin{cases} 1, & d_k \le 1 \\ |\dfrac{tr(U_k)}{tr(W_k)}|, & d_k > 1 \end{cases}$$

where

$$\begin{aligned} U_k &= \hat{R}_k - H_k(P^*_{k|k-1} - K_k P_{zz,k} K_k^T) - \tilde{z}_k \tilde{z}_k^T, \\ W_k &= H_k Q_k H_k^T, \\ d_k &= \frac{tr(\tilde{z}_k \tilde{z}_k^T)}{tr(\hat{R}_k) - H_k P_k H_k^T}. \end{aligned}$$

Proof: The measurement noise covariance matrix R can be adapted based on the residual sequences [38], which is

$$\hat{R}_k = C_{\tilde{z}k} + H_k Q_k H_k^T. \tag{19}$$

We estimate the residual covariance using measurement residuals over m epochs as $C_{\tilde{z}k} = \frac{1}{m} \sum_{i=k-m+1}^{k} \tilde{z}_i \tilde{z}_i^T$, where $\tilde{z}_k = z_k - H_k \hat{x}_k$ denotes the residual sequence. Then, an adaptive scaling factor μ_k is introduced to adjust the process noise covariance Q in real time such that

$$\hat{Q}_k = \mu_k \hat{Q}_{k-1}. \tag{20}$$

According to the definition of residual covariance

$$P_{zz,k} = E[(z_k - \hat{z}_k)(z_k - \hat{z}_k)^T] = C_{\tilde{z}k}, \tag{21}$$

substituting (21) into (19) yields $P_{zz,k} = \hat{R}_k - H_k Q_k H_k^T$. Theoretically, the real filter error $\tilde{z}_k \tilde{z}_k^T$ should be less or equal to the theoretical predication error $\hat{R}_k - H_k Q_k H_k^T$, which is

$$tr(\tilde{z}_k \tilde{z}_k^T) \le tr(\hat{R}_k - H_k Q_k H_k^T). \tag{22}$$

Otherwise, the observer will be in a state of divergence. Thus the process covariance matrix Q should be adjusted by the adaptive factor μ_k. Substituting (8) and (20) into (22) and letting the left and right sides of (22) be equal will result in:

$$\begin{aligned} tr(\tilde{z}_k \tilde{z}_k^T) = tr(\hat{R}_k) - \mu_k tr(H_k Q_k H_k^T) - tr(H_k P^*_{k|k-1} H_k^T) \\ + tr(H_k K_k P_{zz,k} K_k^T H_k^T), \end{aligned}$$

where $P^*_{k|k-1} = P_{k|k-1} - Q_k$. Thus the the adaptive scaling factor μ_k can be calculated as

$$\mu_k = \begin{cases} 1, & d_k \le 1 \\ |\dfrac{tr(U_k)}{tr(W_k)}|, & d_k > 1 \end{cases}$$

where

$$\begin{aligned} U_k &= \hat{R}_k - H_k(P^*_{k|k-1} - K_k P_{zz,k} K_k^T) - \tilde{z}_k \tilde{z}_k^T, \\ W_k &= H_k Q_k H_k^T, \\ d_k &= \frac{tr(\tilde{z}_k \tilde{z}_k^T)}{tr(\hat{R}_k) - H_k Q_k H_k^T}. \end{aligned}$$

■

B. GREEDY GROUPING BASED ON DCR

In order to design l_m optimum tours for MDCs, the set $S = \{s_i^*\}_{1 \le i \le n}$ of collection nodes should be divided into groups G_is such that each Hamilton cycle H_{G_i} is an optimal MDC tour. Because the time gap of visiting the a component twice should be less or equal to that of filling a buffer Buf_{s_i}, which is

$$\frac{L(H_{G_i})}{v} \le \frac{Buf_{s_i^*}}{DCR_{s_i^*}}(1+\theta), \tag{23}$$

where $L(H_{G_i})$ denotes the length of H_{G_i}. Then, the question will be how to construct the optimum grouping $G^* = \{G_i\}$ such that each H_{G_i} will serve as a MDC tour. To this end, a greedy searching algorithm is developed as:

Step 1, construct the H_S using RTPP [22], then each $s_i^* \in H_S$ is numbered sequentially along the H_S, which is $H_S = s_1 s_2 \ldots s_n s_1$ and set $j = 1$ and $G_j = \varnothing$;

Step 2, start with $G_j = s_k, k = j$, repeatedly add s_{k+1} such that $G_j = G_j \cup s_{k+1}$ only if $L(H_{G_j})$ satisfies (23) for each $s_i \in G_j$ and s_{k+1}; then, set $k = k+1$ and repeat this step until each $s_k \in H_S$ belongs to the G_j and set $j = j+1$;

Step 3, repeat step 2 until all $|S|l_k$ groups established, then each grouping G_i^* is determined by:

$$\begin{aligned} G_i^* = \arg\min L(G_i^*) \\ s.t.\ 1.\ G_i^* = \cup G_j, \quad 1 \le j \le |S|l_k; \\ 2.\ \forall G_k, G_j \in G_i^*, \quad G_k \cap G_j = \varnothing. \end{aligned}$$

Among all possible G_i^*s, only the G_i^* with the minimum weight is chosen. We give Theorem 3 for the choice of a proper data loss rate θ.

Theorem 3: If the tolerable data loss rate θ equals to $\max_{G_i \in G^*} \{\frac{1.5L(H^*_{G_i}) \cdot DCR_{s_i^*}}{v \cdot Buf_{s_i^*}} - 1\}$, then we have $AR_{CRrbf} = \frac{1}{1+\theta}$.

Proof: Suppose there exists an optimum algorithm A^* that can discover an optimum grouping G^*. For each group $G_i \in G^*$, if A^* can establish an optimum Hamilton cycle $H^*_{G_i}$ such that

$$\frac{L(H^*_{G_i})}{v} \le \frac{Buf_{s_i^*}}{DCR_{s_i^*}},$$

then there will be no data loss. That implies $AR_{A^*} = 100\%$. Since *RTPP* is a 1.5-approximation algorithm, it will build a H_{G_i} such that $\frac{L(H_{G_i})}{L(H^*_{G_i})} \leq 1.5$. If $\theta = \max_{G_i \in G^*} \{\frac{1.5L(H^*_{G_i})DCR_{s^*_i}}{vBuf_{s^*_i}} - 1\}$, then according to (23) we have

$$\frac{1.5L(H^*_{G_i})}{v} \leq \frac{Buf_{s^*_i}}{DCR_{s^*_i}}(1+\theta).$$

That implies $AR_{CRrbf} = \frac{1}{1+\theta}$.

On the other hand, if we choose $\theta' > \theta$, then $\frac{1.5L(H^*_{G_i})}{v} < \frac{Buf_{s^*_i}}{DCR_{s^*_i}}(1+\theta')$. If we allow each sensor s_i collect data $(1+\theta')$ times of Buf_{s_i}, there are still $\frac{1}{1+\theta}$ data delivered to the sink. Otherwise, we have $\theta' < \theta$ such that $\frac{1.5L(H^*_{G_i})}{v} > \frac{Buf_{s^*_i}}{DCR_{s^*_i}}(1+\theta')$. That implies for each group $G_i \in G^*$ there exists a $G'_i \subset G_i$ such that $\frac{1.5L(H^*_{G'_i})}{v} \leq \frac{Buf_{s^*_i}}{DCR_{s^*_i}}(1+\theta')$. Let each $s_i \in G_i \backslash G'_i$ randomly join a G'_i to establish $G'_{i,new}$ such that $\sum |G'_{i,new}| = n$. It can be verified that $1.5 \leq \frac{L(G'_{i,new})}{L(L(H^*_{G_i}))} \leq 2$. Thus. we have

$$\begin{aligned}\frac{1}{\frac{8}{3}(1+\theta)} &= \frac{Buf_{s^*_i}v}{2DCR_{s^*_i}2L(H^*_{G_i})} \\ &< AR_{CRrbf} \\ &< \frac{Buf_{s^*_i}v}{1.5DCR_{s^*_i}2L(H^*_{G_i})} = \frac{1}{2(1+\theta)}.\end{aligned}$$

Therefore, the theorem holds. ■

The example how the CRrbf restores the connectivity is given in Fig. 2. As shown in Fig. 2(a), there are 10 components C_is that consists of 68 sensors deployed in an area with five different terrains. The set of collection nodes $S = \{s^*_1, s^*_2, \cdots, s^*_{10}\}$ are represented by black dots. In Fig. 2(b), the perfect matches $s^*_2s^*_9$, $s^*_3s^*_{10}$, $s^*_4s^*_5$, and $s^*_7s^*_8$ are added to the mst_S to build an *Ect* first. Then, starting from s^*_1, the $H^d_S = s^*_1s^*_9s^*_2s^*_{10}s^*_3s^*_4s^*_5s^*_6s^*_7s^*_8s^*_1$ is established using *RTPP*. As shown in Fig. 2(c), there exist two optimal grouping G^*_1 and G^*_2 with $E(G^*_2) > E(G^*_1)$. It is clear that G^*_1 is chosen to maximize the aggregation ratio meanwhile reducing the energy cost. In Fig. 2(d), the data of G_1, G_2 and G_3 is collected and eventually delivered to the sink from sinking points s^*_9, s^*_3 and s^*_4 respectively.

C. DISCUSSION

In this Section, we give theoretical analyses on performance advantages of CRrbf in terms of the aggregation ratio, the network latency and network throughput over DBSs and TBSs.

In general, DBSs pursue the travel distance shortening, the load balancing and the latency reducing while TBSs aim to minimize the energy cost, however both of which fail to consider the correlation between the length of a tour, the travelling speed, the buffer size, and the data collection rate. That implies both of DBSs and TBSs can hardly establish

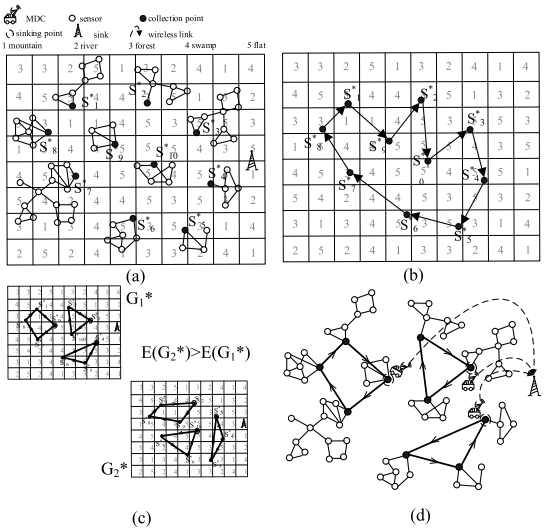

FIGURE 2. The restoration process of CRrbf with $l_m = 3$.

the optimum grouping. With the help of DCRPG, the CRrbf performs better than DBSs and TBSs in the aggregation ratio.

Theorem 4: The aggregation ratio of CRrbf is at least $\frac{1}{4(1+\theta)}$ times greater than that of a DBS or a TBS.

Proof: An algorithm can achieve 100% aggregation ratio only if two following conditions are satisfied:

1. discovering the G^*;
2. building $H^*_{G_i}$ for each $G_i \in G^*$.

Then, we are going to distinguish three cases to prove this theorem.

Case 1: ∀DBSs and TBSs satisfying condition 1 only.

According to Theorem 3, we have

$$\begin{aligned}AR_{CRrbf} &= \frac{1}{1+\theta} = \frac{Buf_{s^*_i}v}{DCR_{s^*_i}1.5L(H^*_{G_i})}, \\ \frac{AR_{DBS}}{AR_{CRrbf}} &= \frac{3}{4(1+\theta)}, \\ \frac{AR_{TBS}}{AR_{CRrbf}} &< \frac{3}{4(1+\theta)}.\end{aligned}$$

Case 2: ∀DBSs and TBSs satisfying condition 2 only.

In this case, if DBSs employ *RTPP*, then we have

$$AR_{TBS} < AR_{DBS} < \frac{Buf_{s^*_i}v}{DCR_{s^*_i}1.5\lambda L(H^*_{G_i})} = \frac{1}{\lambda(1+\theta)},$$

where λ denotes the ratio between the length of an suboptimal grouping established by DBSs or TBSs and that of the optimal one with $2 \geq \lambda \geq 1.5$.

Case 3: ∀DBSs and TBSs satisfying neither condition 1 nor 2.

It can be deduced that $AR_{TBS} < AR_{DBS} < \frac{1}{\frac{4\lambda}{3}(1+\theta)}$. ■

A a DBS, the CISIL establishes l_m triangles as MDC tours. That implies there are only $3l_m$ sensors visited by MDCs. For each group $G_i \in G^*$ satisfying constrain (23), it is easy to get $AR_{CISIL} = \frac{1}{\frac{n}{3l_m}(1+\theta)} < \frac{1}{\frac{4}{3}(1+\theta)}$ due to $n \gg l_m$. As a TBS,

TABLE 3. Simulation setup.

Parameter	*Description*	*Value*
Area	Area of interest	1000 m×1000 m
v	MDC Speed	[20, 90] km/h
N	Number of nodes	[100, 240]
DCR	Data Collection Rate	[80,220] bit/s
$Buf_{.}$	Buffer size	2Mbit
l_m	Number of MDC	[4,11]
n	Number of Components	[1,8]
θ	Tolerable Data Lost Rate	[0.05,0.225]
k	Constant Coefficient	10^{-4} joule/meter^2
c	Energy Coefficient	30 joule/meter

the ReBAT is 3.1-approximation algorithm while the approximation ratio of HRSRT is 2.325 in terms of energy cost [22]. It can be deduced that $AR_{ReBAT} = \frac{1}{\frac{3.1}{\alpha}(1+\theta)}$ and $AR_{HRSRT} = \frac{1}{\frac{2.325}{\alpha}(1+\theta)}$, where $\alpha = \frac{Buf_{s_i} v^2 crisk_{min} elevation_{min}(1+\theta)}{DCR_{s_i} E^*} < 1$.

Theorem 5: The complexity of CRrbf is $O(n^2 \log n!)$.

Proof: It is evident that the complexity of CRrbf depends on DCR based greedy grouping that partitions the set of collection points into l_m groups G_is based on the DCR prediction. If for each G_i we have $|G_i| \geq 3$, then there exists a group G_j such that $|G_j| \leq n - 3(l_m - 1)$. Because DCRPG builds each G_i in a greedy searching manner such that a sensor s_i can join the G_i only if $H_{G_i \cup \{s_i\}}$ satisfies the constrain (23). That implies the complexity of the greedy searching process is no more than $\sum_{i=1}^{\mathsf{n}} i \log i$, where $\mathsf{n} = n - 3(l_m - 1)$. In addition, the RTPP employed by DCRPG is responsible for the construction of Hamilton cycles, the complexity of which is $O(n \log n)$ [22]. Therefore, the complexity of CRrbf is $O\left(n^2 \log n!\right)$. ■

In fact, CRrbf outperforms both DBSs and TBSs not only in the aggregation ratio, but the network latency and network throughput as well. The reasons are as follows. Consider the same tolerable data loss rate while compared with both of DBSs and TBSs, it is obviously that the network latency depends on the transmission latency in our scenario. According to Theorem 3, we know that CRrbf constructs a MDC tour as long as 3/4 of that of any DBSs or TBSs. Given the same MDC velocity, it can be deduced that the network latency of CRrbf is only 3/4 of that of a DBS or a TBS. On the other hand, the definition of the aggregation ratio and Theorem 3 guarantee that the network throughput of CRrbf is at least $\frac{1}{4(1+\theta)}$ times greater than that of any DBSs or TBSs.

IV. VALIDATION EXPERIMENT

1) EXPERIMENT SETUP, PERFORMANCE METRICS AND BASELINE APPROACHES

The performance of CRrbf has been validated through extensive simulation experiments which are developed in Python on an Intel Core i5-8250U 1.6 GHZ CPU, 8GB RAM computer. Simulation parameters are given in Table 3.

Eq. (1)∼(7) are employed to calculate the energy cost, where c is proportional to v referring the cost for movement per meter on a flat topology which is taken as 30 $joule/meter$, the constant coefficient $k = 10^{-4}$ $joule/meter^2$ and the risks and elevations of corresponding terrains are listed in Table 4.

TABLE 4. Terrain types, risk rates, and elevation.

Type	*Risk*	*Elevation*
Swamp	0.05	(0,1]
Mountain	0.004	(0,5]
River	1	(0,1]
Forest	0.002	(0,3]
Flat	0.001	1

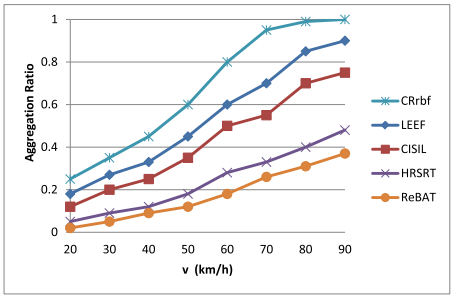

FIGURE 3. The aggregation ratio comparison while varying v.

We compare CRrbf with baseline approaches LEEF [15], CISIL [14], HRSRT [22] and ReBAT [23] in terms of aggregation ratio, energy cost and maximum energy cost while varying MDC count (l_m), velocity (v), number of components (n), number of nodes (N), data collection rate (DCR), and tolerable data loss rate (θ).

2) SIMULATION RESULTS

The results of individual experiments for 50 topologies are averaged with simulation setup given in Table3.

As shown in Fig. 3, the aggregation ratio grows rapidly at the beginning with v and eventually levels off for all strategies. It is obvious that CRrbf achieves the highest aggregation ratio. The reason for that is the CRrbf exploits the optimum grouping of sensors based on the DCR prediction and the 1.5-approximation Hamilton cycle construction algorithm for the MDC tour design while DBSs and TBSs can hardly establish the optimum MDC tour without the DCR prediction.

The adverse impact on the aggregation ratio is shown in Fig. 4. It is clear that the aggregation ratio drops as n increases and eventually gets stable for all strategies. The reason for that is as follows. The traveling distance increase with more components involved such that more data is lost at the beginning. However, the distance between each pair of components grows slowly while the deployment area is densely populated eventually. It is clear that the CRrbf still performs the best among all.

Fig. 5 gives the performance comparison with the growth of DCR which is one of many dominant factors that directly affect the aggregation ratio for all strategies. As we explain before, the DCR should be chosen carefully to maintain the aggregation ratio. That implies if the DCR is larger than a threshold, than the aggregation ratio drops quickly. It is

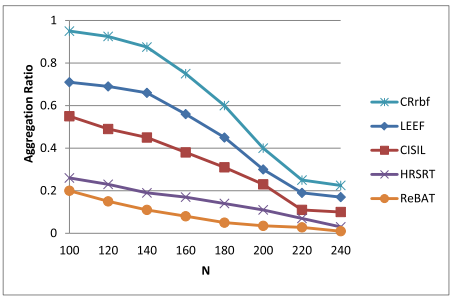

FIGURE 4. The aggregation ratio comparison while varying N.

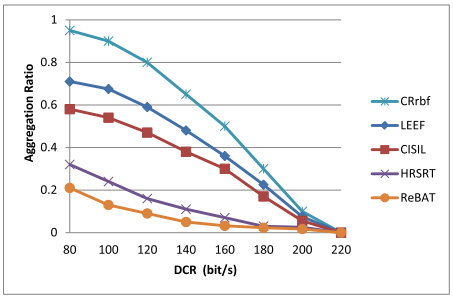

FIGURE 5. The aggregation ratio comparison while varying DCR.

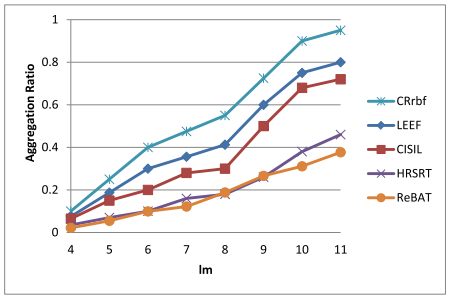

FIGURE 6. The aggregation ratio comparison while varying l_m.

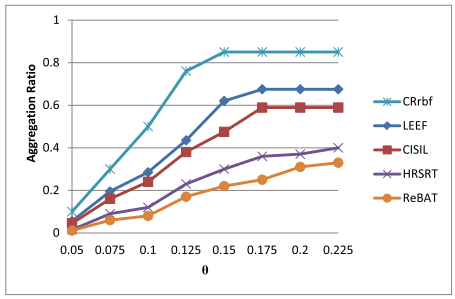

FIGURE 7. The aggregation ratio comparison while varying θ.

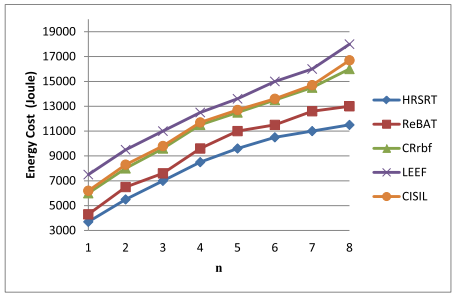

FIGURE 8. The energy cost comparison while varying n.

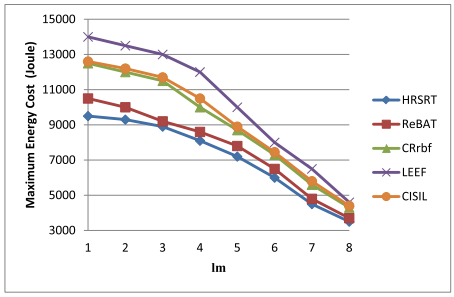

FIGURE 9. The maximum energy cost comparison while varying l_m.

obvious that all strategies achieve the highest aggregation ratios respectively with DCR=80bit/s compared with the lowest ones while the DCR reaches 220bit/s. Even if the aggregation ratio drops rapidly, the CRrbf still maintains the highest one.

As shown in Fig. 6, all aggregation ratios rise with l_m and tend to be stable at last. This is because the more MDCs join the data collection the less data is lost. However the deployment area is bounded, if l_m is sufficient then the aggregation ratio will reach 100% such that no more extra MDCs are required. Once again, no matter how many MDCs available, the CRrbf still maintains the highest aggregation ratio.

Fig. 7 shows the performance comparison with the growth of θ. Similar to the DCR, the θ is another dominant factor while determining the aggregation ratio. Obviously, all aggregation ratios increase as the θ, while $\theta \geq 0.15$ the aggregation ratios begin to level off. Note that the CRrbf not only accomplishes the highest aggregation ratio but becomes the first one to converge as well.

It can be observed from Fig. 8 that each approach consumes more energy as n increases with $l_m = 11$. Although the CRrbf consumes more energy than HRSRT and ReBAT, it performs better than LEEF and CISIL. The reason for that is although more components are involved, the energy cost is no longer increased rapidly due to the optimum tour design. In Fig. 9, it is clear that the maximum energy cost for each strategy drops as l_m increases. The CRrbf outperforms all DBSs.

V. RELATED WORKS

There exist two categories of connectivity restoration strategies, which is initially designed based on wireless networks.

The strategies that that focus on either travel distance, load balance, latency, throughput or energy cost is called DBSs in this paper. In [18], Abbas and Younis design the MIMSI. It first partitions the component set into convex hulls, among which a minimum spanning tree is built for inter-partition connection. Then collection sensors are selected utilizing the center of mass to discover optimal tours, each of which is

designated a MDC. Eventually, the connectivity is restored by deploying relay nodes between MDC tours. Similar to MIMSI, the RCR [16] further shortens the MDC tours by deploying relay devices. In [20], Stanislaus and Younis develop a delay-conscious recovery strategy FeSMoR, which chooses round trips and steiner triangles as MDC tours with relay devices to provide tour connection. The IDM-kMDC is developed in [21]. First, MDC tours are formed along the convex polygon of components with collection sensors located utilizing the center of mass. Once again, optimal k tours are established by emerging MDC tours. In [17], MINDS is designed to minimize total tour length but balance the load equitably among MDCs as well. The ToCS [19] attempts to reduce the latency by finding the balanced tour paths among MDCs. It first utilizes a star topology for component grouping, and then the MDC tours are equalized by adjusting the size of the cluster. Recently, CISIL [14] is develop by exploiting the Delaunay triangulation for node set partition, in which k 3-hyperedges of the 3-hypergraph are chosen as final MDC tours. Note that CRrbf also takes the periphery of each component into consideration in order to choose the proper collection sensors due to the fact that the optimization of the candidate selection for collection sensors will significantly shorten MDC tours. The LEEF [15] is designed to equalize the energy cost, which is quantified by cell-based grid with respect to motion and wireless communication, consumed by k MDCs through greedy expansion and optimization successively. Although shortening MDC tours will somehow increase the aggregation ratio, the data collection rate, the buffer size and the speed that could potentially affect the aggregation ratio exploited by CRrbf are neglected by DBSs. Note that the energy cost is another concern. In [27], stochastic geometry is used to design a relay-based connectivity recovery scheme for a wireless sensor network whose the goal is to optimize the tradeoff between the number of selected relays and the energy spent to restore connectivity. The work in [28] proposes a dynamic clustering and routing algorithm to maintain connectivity and achieve energy efficiency in a large scale sensor network. Although the energy cost is distance-related, terrains can affect the energy cost even more in realistic environments.

The other strategies that consider terrain influences in realistic environments is called TBS in this paper. In [23], Senturk *et al.* develop the ReBAT that applies a grid based mapping to quantify the terrain in order to locate the least energy cost paths for connectivity restoration. However, ReBAT only ensures the network to be 1-connected. Wang *et al.* [22] design a hybrid restoration strategy to achieve 2-connectivity based on random terrains. In [26], Zhou *et al.* propose a rapidly exploring random tree based algorithm to find paths with the least cost for obstacle avoidance and component connection. Truong *et al.* [24] consider how obstacles affect the mobility and communication of relay devices for the minimization of agents' mobility cost. Mi *et al.* [25] investigate how to avoid convex obstacles and inter-sensor collisions during connectivity restoration. Although TBSs can reduce the energy cost efficiently, the aggregation ratio is disregarded while compared with the proposed strategy CRrbf.

VI. CONCLUSION

In this paper, the connectivity reconstruction problem for IIoTs is considered. A machine learning based strategy CRrbf, that utilizes a Radial Basis Function Neural Network (RBFNN) along with an Unscented Kalman Filter (UKF), is proposed to maximize the aggregation ratio and reduce the energy cost as well during the connectivity restoration. Be specific, CRrbf deploys MDCs to provide intermitted connections between separated components for data collection and aggregation. The MDC tour design by CRrbf integrates buffer size, data collection rate, tolerable data loss rate, travel speed and terrain influence such that the aggregation ratio is significantly increased meanwhile the energy cost is reduced. The theoretical analysis and simulations results show that the aggregation ratio of CRrbf outperforms both distance based strategies and terrain based strategies in terms of the sinking ratio, the network latency and the throughput.

Our future works include the connectivity restoration for IIoTs with only a limited number of relay nodes and mobile data collectors available. In addition, an efficient mobile data collector tour by exploiting a deep reinforcement learning, i.e., DDPG, is one of our future interests.

REFERENCES

[1] S. Mumtaz, A. Alsohaily, Z. Pang, A. Rayes, K. F. Tsang, and J. Rodriguez, "Massive Internet of Things for industrial applications: Addressing wireless IIoT connectivity challenges and ecosystem fragmentation," *IEEE Ind. Electron. Mag.*, vol. 11, no. 1, pp. 28–33, Mar. 2017.

[2] J. A. Stankovic, "Research directions for the Internet of Things," *IEEE Internet Things J.*, vol. 1, no. 1, pp. 3–9, Feb. 2014.

[3] K. Wang, Y. Shao, L. Shu, C. Zhu, and Y. Zhang, "Mobile big data fault-tolerant processing for ehealth networks," *IEEE Netw.*, vol. 30, no. 1, pp. 36–42, Jan. 2016.

[4] B. Kantarci and H. T. Mouftah, "Mobility-aware trustworthy crowdsourcing in cloud-centric Internet of Things," in *Proc. IEEE Symp. Comput. Commun. (ISCC)*, Jun. 2014, pp. 30–36.

[5] K. Wang, Y. Wang, Y. Sun, S. Guo, and J. Wu, "Green industrial Internet of Things architecture: An energy-efficient perspective," *IEEE Commun. Mag.*, vol. 54, no. 12, pp. 48–54, Dec. 2016.

[6] X. He, K. Wang, and W. Xu, "QoE-driven content-centric caching with deep reinforcement learning in edge-enabled IoT," *IEEE Comput. Intell. Mag.*, vol. 14, no. 4, pp. 12–20, Nov. 2019.

[7] S. Al-Sarawi, M. Anbar, K. Alieyan, and M. Alzubaidi, "Internet of Things (IoT) communication protocols: Review," in *Proc. 8th Int. Conf. Inf. Technol. (ICIT)*, Amman, Jordan, May 2017, pp. 685–690.

[8] K. E. Nolan, W. Guibene, and M. Y. Kelly, "An evaluation of low power wide area network technologies for the Internet of Things," in *Proc. Int. Wireless Commun. Mobile Comput. Conf. (IWCMC)*, Paphos, Cyprus, Sep. 2016, pp. 439–444.

[9] M. De Sanctis, E. Cianca, G. Araniti, I. Bisio, and R. Prasad, "Satellite communications supporting Internet of remote things," *IEEE Internet Things J.*, vol. 3, no. 1, pp. 113–123, Feb. 2016.

[10] M. Tanha, D. Sajjadi, F. Tong, and J. Pan, "Disaster management and response for modern cellular networks using flow-based multi-hop Device-to-Device communications," in *Proc. IEEE 84th Veh. Technol. Conf. (VTC-Fall)*, Montreal, QC, Canada, Sep. 2016, pp. 1–7.

[11] M. J. Farooq and Q. Zhu, "Secure and reconfigurable network design for critical information dissemination in the Internet of battlefield Things (IoBT)," in *Proc. 15th Int. Symp. Model. Optim. Mobile, Ad Hoc, Wireless Netw. (WiOpt)*, Paris, France, May 2017, pp. 1–8.

[12] M. J. Farooq and Q. Zhu, "On the secure and reconfigurable multi-layer network design for critical information dissemination in the Internet of battlefield Things (IoBT)," *IEEE Trans. Wireless Commun.*, vol. 17, no. 4, pp. 2618–2632, Apr. 2018.

[13] J. Liu, H. Shen, L. Yu, H. S. Narman, J. Zhai, J. O. Hallstrom, and Y. He, "Characterizing data deliverability of greedy routing in wireless sensor networks," *IEEE Trans. Mobile Comput.*, vol. 17, no. 3, pp. 543–559, Mar. 2018.

[14] W. Lalouani, M. Younis, and N. Badache, "Interconnecting isolated network segments through intermittent links," *J. Netw. Comput. Appl.*, vol. 108, pp. 53–63, Apr. 2018.

[15] S. Lee, M. Younis, B. Anglin, and M. Lee, "LEEF: Latency and energy efficient federation of disjoint wireless sensor segments," *Ad Hoc Netw.*, vol. 71, pp. 88–103, Mar. 2018.

[16] Y. K. Joshi and M. Younis, "Restoring connectivity in a resource constrained WSN," *J. Netw. Comput. Appl.*, vol. 66, pp. 151–165, May 2016.

[17] Y. K. Joshi and M. Younis, "Mobility-based Internetworking of disjoint segments," in *Proc. 27th Biennial Symp. Commun. (QBSC)*, Jun. 2014, pp. 193–197.

[18] A. Abbas and M. Younis, "Establishing connectivity among disjoint terminals using a mix of stationary and mobile relays," *Comput. Commun.*, vol. 36, no. 13, pp. 1411–1421, Jul. 2013.

[19] J. L. V. M. Stanislaus and M. Younis, "Mobile relays based federation of multiple wireless sensor network segments with reduced-latency," in *Proc. IEEE Int. Conf. Commun. (ICC)*, Jun. 2013, pp. 6407–6411.

[20] J. L. V. M. Stanislaus and M. Younis, "Delay-conscious federation of multiple wireless sensor network segments using mobile relays," in *Proc. IEEE Veh. Technol. Conf. (VTC Fall)*, Sep. 2012, pp. 1–5.

[21] F. Senel and M. Younis, "Optimized interconnection of disjoint wireless sensor network segments using k mobile data collectors," in *Proc. IEEE Int. Conf. Commun. (ICC)*, Jun. 2012, pp. 492–496.

[22] X. Wang, L. Xu, S. Zhou, and W. Wu, "Hybrid recovery strategy based on random terrain in wireless sensor networks," *Scientific Program.*, vol. 2017, pp. 1–19, 2017.article id. 5807289

[23] I. F. Senturk, K. Akkaya, and S. Janansefat, "Towards realistic connectivity restoration in partitioned mobile sensor networks," *Int. J. Commun. Syst.*, vol. 29, no. 2, pp. 230–250, Jan. 2016.

[24] T. T. Truong, K. N. Brown, and C. J. Sreenan, "Multi-objective hierarchical algorithms for restoring wireless sensor network connectivity in known environments," *Ad Hoc Netw.*, vol. 33, pp. 190–208, Oct. 2015.

[25] Z. Mi, Y. Yang, and J. Y. Yang, "Restoring connectivity of mobile robotic sensor networks while avoiding obstacles," *IEEE Sensors J.*, vol. 15, no. 8, pp. 4640–4650, Aug. 2015.

[26] S. Zhou, M.-Y. Wu, and W. Shu, "Terrain-constrained mobile sensor networks," in *Proc. IEEE Global Telecommun. Conf.*, 2005. vol. 1, p. 5.

[27] L. Goratti, T. Baykas, T. Rasheed, and S. Kato, "NACRP: A connectivity protocol for star topology wireless sensor networks," *IEEE Wireless Commun. Lett.*, vol. 5, no. 2, pp. 120–123, Apr. 2016.

[28] Z. Xu, L. Chen, C. Chen, and X. Guan, "Joint clustering and routing design for reliable and efficient data collection in large-scale wireless sensor networks," *IEEE Internet Things J.*, vol. 3, no. 4, pp. 520–532, Aug. 2016.

[29] X. He, K. Wang, H. Huang, T. Miyazaki, Y. Wang, and S. Guo, "Green resource allocation based on deep reinforcement learning in content-centric IoT," *IEEE Trans. Emerg. Topics Comput.*, early access, Feb. 13, 2018, doi: 10.1109/TETC.2018.2805718.

[30] K. Wang, Y. Shao, L. Xie, J. Wu, and S. Guo, "Adaptive and fault-tolerant data processing in healthcare IoT based on fog computing," *IEEE Trans. Netw. Sci. Eng.*, vol. 7, no. 1, pp. 263–273, Jan. 2020, doi: 10.1109/TNSE.2018.2859307.

[31] C. Xu, K. Wang, Y. Sun, S. Guo, and A. Y. Zomaya, "Redundancy avoidance for big data in data centers: A conventional neural network approach," *IEEE Trans. Netw. Sci. Eng.*, vol. 7, no. 1, pp. 104–114, Jan. 2020, doi: 10.1109/TNSE.2018.2843326.

[32] X. He, K. Wang, H. Huang, and B. Liu, "QoE-driven big data architecture for smart city," *IEEE Commun. Mag.*, vol. 56, no. 2, pp. 88–93, Feb. 2018.

[33] K. Wang, C. Xu, Y. Zhang, S. Guo, and A. Y. Zomaya, "Robust big data analytics for electricity price forecasting in the smart grid," *IEEE Trans. Big Data*, vol. 5, no. 1, pp. 34–45, Mar. 2019.

[34] G. Robins and A. Zelikovsky, "Tighter bounds for graph steiner tree approximation," *SIAM J. Discrete Math.*, vol. 19, no. 1, pp. 122–134, Jan. 2005.

[35] D. Chen, D.-Z. Du, X.-D. Hu, G.-H. Lin, L. Wang, and G. Xue, "Approximations for steiner trees with minimum number of steiner points," *Theor. Comput. Sci.*, vol. 262, nos. 1–2, pp. 83–99, Jul. 2001.

[36] D. Z. Du and F. K. Hwang, "The state of art on Steiner ratio problems," *Comput. Euclidean Geometry*, Jun. 1992, Art. no. 163191, doi: 10.1142/9789814355858_0005.

[37] D. H. Zhou and P. M. Frank, "Strong tracking filtering of nonlinear time-varying stochastic systems with coloured noise: Application to parameter estimation and empirical robustness analysis," *Int. J. Control*, vol. 65, no. 2, pp. 295–307, Sep. 1996.

[38] J. Wang, "Stochastic modeling for real-time kinematic GPS/GLONASS positioning," *Navigation*, vol. 46, no. 4, pp. 297–305, Dec. 1999.

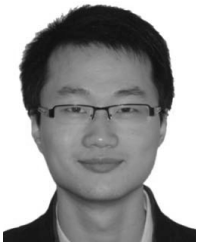

JIONG WANG received the M.S. degree in computer technology from Fuzhou University, China, in 2011. He is currently a Senior Engineer with the College of Computer and Control Engineering, Minjiang University, Fuzhou, China. His research interests include wireless sensor networks and network security.

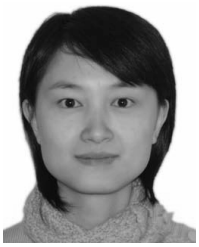

HUA ZHANG received the M.S. degree in computer technology from Fuzhou University, China, in 2011. She is currently a Lecturer with the College of Computer and Control Engineering, Minjiang University, Fuzhou, China. Her research interests include computer networks and information security.

ZHIQIANG RUAN received the B.S. degree from Fujian Normal University, China, in 2006, and the M.S. and Ph.D. degrees from Hunan University, China, in 2009 and 2012, respectively, all in computer science. He is currently an Associate Professor with the College of Computer and Control Engineering, Minjiang University, China. His research interests include resource optimization and management, communication and energy systems, network security, and its applications.

TAO WANG received the B.E. degree in information engineering from the South China University of Technology, Guangzhou, China, in 2009, and the Ph.D. degree in computer science from The Australian National University, Canberra, ACT, Australia, in 2016. He was a member of the Computer Vision Research Group, National ICT Australia, Canberra. He is currently a Lecturer with the College of Computer and Control Engineering, Minjiang University, Fuzhou, China. His research interests include scene understanding and deep learning.

XIAODING WANG received the Ph.D. degree from the College of Mathematics and Informatics, Fujian Normal University, China, in 2016. He is currently an Associate Professor with Fujian Normal University. His main research interests include network optimization and fault tolerance.